Research Square

Preprints are preliminary reports that have not undergone peer review.
They should not be considered conclusive, used to inform clinical practice,
or referenced by the media as validated information.

Electromagnetic Modeling of a Phase-Shifting Transformer Based on DC Hysteresis Measurements

Alexander Fröhlich

a.froehlich@tugraz.at

Graz University of Technology

Dennis Albert

OMICRON electronics

Tomasz Bednarczyk

OMICRON electronics

Sergey Zirka

Dnipro National University

Gerald Leber

Siemens Energy Austria

Herwig Renner

Graz University of Technology

Research Article

Keywords: phase-shifting transformers, DC hysteresis, electromagnetic modeling, topological model

Posted Date: July 20th, 2026

DOI: https://doi.org/10.21203/rs.3.rs-10206171/v1

License: This work is licensed under a Creative Commons Attribution 4.0 International License.
Read Full License

Additional Declarations: No competing interests reported.

Electromagnetic Modeling of a Phase-Shifting Transformer Based on DC Hysteresis Measurements

Alexander Fröhlich[1*], Dennis Albert[2], Tomasz Bednarczyk[2], Sergey Zirka[3], Gerald Leber[4] and Herwig Renner[1]

[1*]Graz University of Technology, Institute of Electrical Power Systems, Graz, Austria
[2]OMICRON electronics, Klaus, Austria
[3]Dnipro National University, Dnipro, Ukraine
[4]Siemens Energy Austria, Weiz, Austria

*Corresponding author: a.froehlich@tugraz.at, 10009-0009-2414-6956;
Contributing authors: dennis.albert@omicronenergy.com, 0000-0001-8916-851X;
tomasz.bednarczyk@omicronenergy.com; 0000-0001-6762-0050;
zirka@email.dp.ua, 0000-0001-7607-1436;
gerald.leber@siemens-energy.com;
herwig.renner@tugraz.at, 0000-0002-5471-9198;

Abstract

This paper presents an electromagnetic modeling methodology for a 600 MVA phase-shifting transformer, developed using limited manufacturer design data combined with DC hysteresis measurements. Phase-shifting transformers play a critical role in controlling active power flow within interconnected power systems, yet their accurate representation for transient studies remains challenging due to restricted access to detailed design information, particularly for units already in service. To address this, both saturation-based and hysteresis-based modeling approaches are formulated and parameterized from experimentally obtained DC hysteresis loops. The transformer is also modelled in ATPDraw using a dynamic hysteresis model with prescribed core materials, enabling an accurate representation of nonlinear magnetic characteristics. The proposed models are validated against factory acceptance test results, showing good agreement across the relevant operating conditions. Furthermore, the model is independently verified through implementation in RelaySimTest software, confirming its suitability for low-frequency transient analysis and protection studies. The results demonstrate that DC hysteresis measurements provide an effective basis for transformer parameterization, enabling accurate reproduction of the nonlinear magnetic behavior.

Keywords*:* phase-shifting transformers, DC hysteresis, electromagnetic modeling, topological model

1. INTRODUCTION

Accurate electromagnetic modeling of phase-shifting transformers (PST) is essential for analyzing low-frequency transients (phenomena covering frequencies below the first resonance [1]) in power systems, such as inrush currents, short-circuit (SC) events, ferroresonances, harmonics, and geomagnetically induced currents. However, access to detailed design specifications is often limited, especially for in-service equipment. This study investigates alternative modeling techniques that require minimal input data. Using a 600 MVA PST as a case study, we explore the application of DC hysteresis measurements to parametrize both saturation and hysteresis-based models. The approach leverages factory acceptance test (FAT) data and on-site measurements to build reliable models suited for transient simulations, demonstrating that effective modeling is possible even when full manufacturer data is unavailable. Both models are verified using FAT results and further validated through a second simulation in RelaySimTest (RST) software, confirming their accuracy and applicability in practical protection studies.

2. DC HYSTERESIS

To accurately validate electromagnetic models during transient system studies, specific data regarding transformer saturation is essential. In practice, only terminal currents can be measured, and these differ significantly from the internal magnetizing currents within the transformer legs [2]. This discrepancy is caused by several factors, including magnetic coupling between the phases, the magnetizing current of the yokes, and the capacitances of the windings and bushings.

Accurately representing non-linear core behavior up to deep saturation is particularly difficult when specific material data are unavailable. A major challenge is that the magnetizing current in one phase is directly influenced by the processes occurring in the other phases. Consequently, standard three-phase measurements cannot be used to extract a single hysteresis characteristic for the entire core due to this inter-phase magnetic coupling. To address this issue, a saturation test was conducted on the 600 MVA PST, as shown in Fig. 2. By applying a single-phase voltage between the high voltage series terminals S1 - S3, the magnetic flux in the middle leg is cancelled out, reducing inter-phase coupling to a minimum [3], as depicted in Fig. 1.
Although these tests are typically performed at a rated frequency of 50 Hz, the voltage required to reach deep saturation often exceeds the transformer's insulation limits. To safely achieve deep saturation, the frequency was reduced, leading to the use of a DC voltage with alternating polarity. This DC hysteresis test offers two main practical advantages:

- The test can be performed using a small portable testing device, due to the lower power requirements.
- Reducing the frequency prevents high magnetizing current demands, which in turn lowers the power demand on the testing equipment.

The waveforms captured during the DC hysteresis test are illustrated in Fig. 3. These readings form the basis for the hysteresis curve. To refine this data, the resistive voltage drop across the windings is first calculated and removed from the terminal voltage measurements. The resulting loop (purple curve in Fig. 4) is then centered around the vertical axis. To finalize the model parameters, the ascending and descending branches of this loop are consolidated into a single, continuous saturation curve (blue curve in Fig. 4).

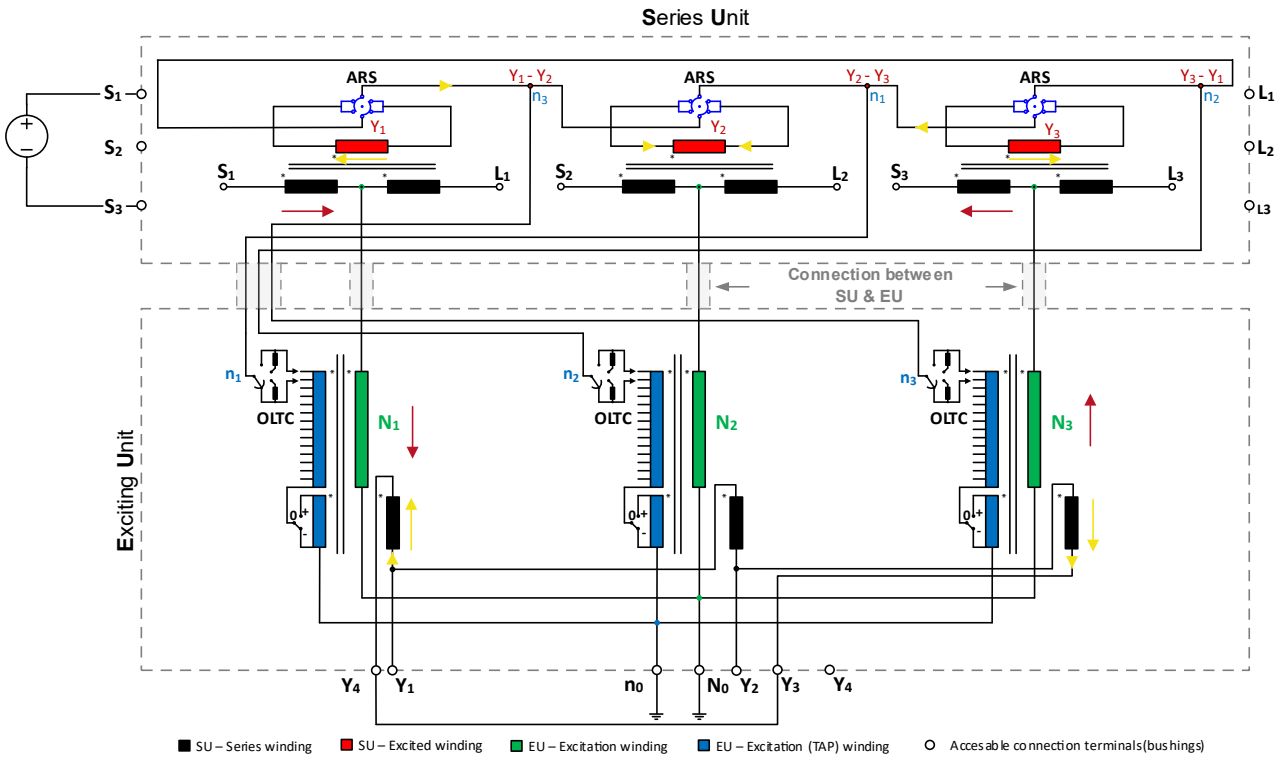


Fig. 1: DC hysteresis measurement setup between terminals S1 and S3 with OLTC in neutral position. Red arrows: induced flux by DC hysteresis measurement; Yellow arrows: vanishing flux and current in booster winding and tertiary delta winding.



Fig. 2: On-site factory DC hysteresis measurement of the SU-PST.

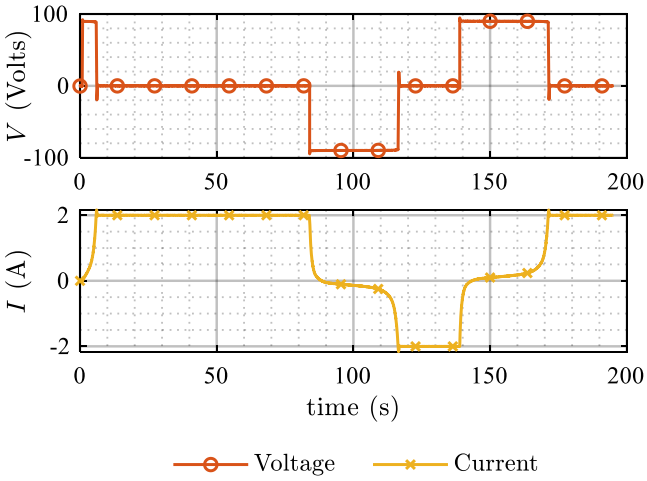


Fig. 3: Voltage and current values recorded at the S terminals (S1-S3) throughout the transformer's DC hysteresis measurement.

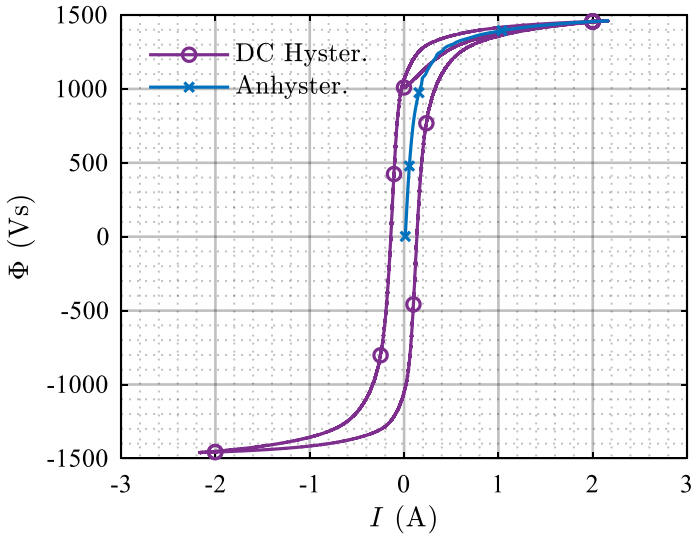


Fig. 4: Measured DC hysteresis loop at S-terminals (S1-S3) and calculated anhysteretic curve.

3. TOPOLOGY MODELING APPROACH

The PST under investigation is a symmetrical two-core two-tank device consisting of the Series Unit (SU) and Exciting Unit (EU). To obtain a pure electrical model of the PST, the five-legged transformers of the SU and EU should be represented by their electrical equivalents. A widely used approach for converting a magnetic model into its electrical counterpart is the application of the duality transformation [4].

The following nomenclature is used throughout this document. TABLE 1 summarizes the designations and functional descriptions for the winding components of both the SU and EU. The winding configurations of the SU and EU are illustrated in Fig. 1 and Fig. 7, which also depict the center-tapped sections (S & L) of the SU connected to the EU.

TABLE 1: DEFINITIONS AND ABBREVIATIONS FOR SERIES UNIT (SU) AND EXCITING UNIT (EU) WINDINGS.

	Code	Winding	Description
Series Unit (SU)	SW	Series	Two sections (S & L), center-tapped to the exciting unit.
	EWS	Excited	Comprises four dedicated winding sections (EWS1i, EWS2i, EWS1o, EWS2o).
Exciting Unit (EU)	EW	Exciting	Main electrical connection to the series unit.
	CW	Coarse	98 turns; in-phase (advanced) or 180° shift (retard).
	FW	Fine	Incremental regulation via 7 turns per step.
	TW	Tertiary	Delta winding; used for NL test energization at FAT.

Fig. 5 shows the duality-derived model of the PST, connected to the supply side through terminals S1, S2, and S3, and to the load side via terminals L1, L2, and L3. The transformer models in Fig. 5 reproduce the topology of their cores and windings. The wound core legs are represented by the hysteretic inductors L_A, L_B, and L_C. Inductors L_{AB} and L_{BC} represent the yokes, while inductors L_{AA} and L_{CC} correspond to the outer legs and the adjoining core yokes. Air gaps at the core joints, when considered, are represented by inductances L_G, which may be linear or non-linear [5].

If the hysteretic inductors are static, such as in the JA model, they are shunted by appropriate loss resistors (not shown in Fig. 5). Since both active parts employ five-legged cores, the magnetic flux hardly penetrates the magnetic shields and tank walls [6, 7]. Consequently, these structural components are omitted in the duality-based models employed.
The zero-sequence impedance per phase is denoted as L_0. As outlined in [7], concentrating the zero-sequence impedance in the central leg reduces the saturation inductance of the yoke, resulting in an increased magnetizing current at elevated flux densities.

In the SU leakage model in Fig. 6a), the identical sections S and L of the SW (145 turns each) are represented as separate windings, denoted as windings 1 and 2, respectively. They are symmetrically arranged with respect to coil 3 (486 turns) of the delta winding. Therefore, the three windings of the SU transformer are characterized by two leakage inductances: L_{s12}, representing the leakage between windings 1 and 2, and L_{s13}, representing the leakage between winding 1 (or 2) and winding 3. The leakage model of the three windings is shown in Fig. 6b), where $L_2 = L_{s12}/2$ and $L_{p1} = L_{s13} - L_{s12}/2$. The inductance between nodes 1-2 equals L_{s12}, whereas the inductance between nodes 1-3 and nodes 2-3 both equal L_{s13}. The considered leakage structure can be incorporated into the SU model, as shown in Fig. 6c), where phase A is taken as an example. The values L_2 and L_{p1} are determined by numerical experiments on the PST short-circuit test with the on-load tap-changer (OLTC) in the neutral position.

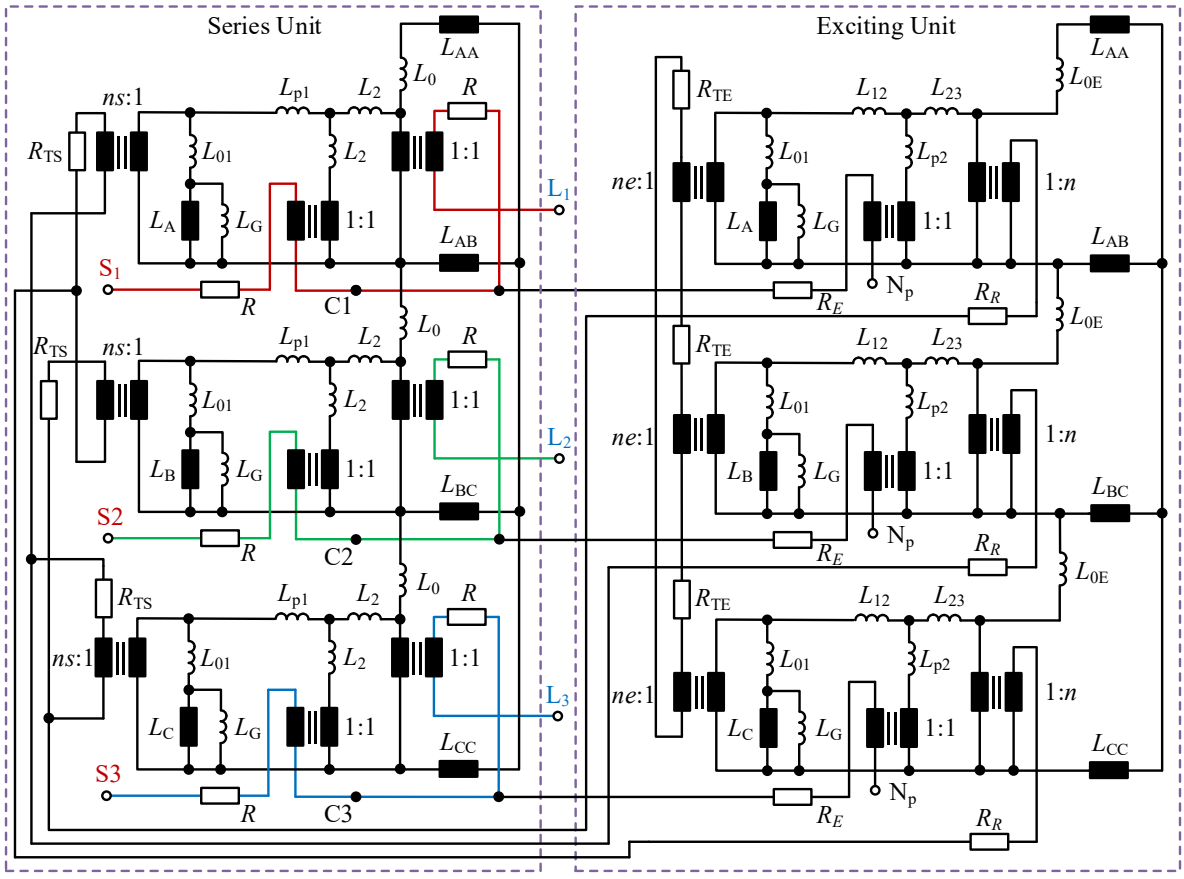


Fig. 5: Topology-based model of the three winding five-legged SU and EU of the YNyn/IIId PST. The magnetic core characteristics are represented by non-linear hysteretic inductors (black rectangles), while linear inductances are represented by wavy symbols. The components labelled 1:1 represent ideal transformers.

The three (presumably concentric) windings of the EU transformer are characterized by the leakage inductances L_{s12E}, L_{s23E} and L_{s13E}, where the suffix "E" denotes the EU unit. For concentric windings, it is typical that $L_{s13E} > L_{s12E} + L_{s23E}$. To reproduce the measured (or calculated) inductances L_{s12E}, L_{s23E}, and L_{s13E}, it is convenient to introduce a parameter $L_{pE} = (L_{s13E} - L_{s12E} - L_{s23E}) / 2$ [7]. Then, the per-phase leakage models of the EU transformer can be represented as shown in Fig. 5, where $L_{12} = L_{s12E} + L_{pE}$, $L_{23} = L_{s23E} + L_{pE}$, and $L_{p2} = -L_{pE}$.

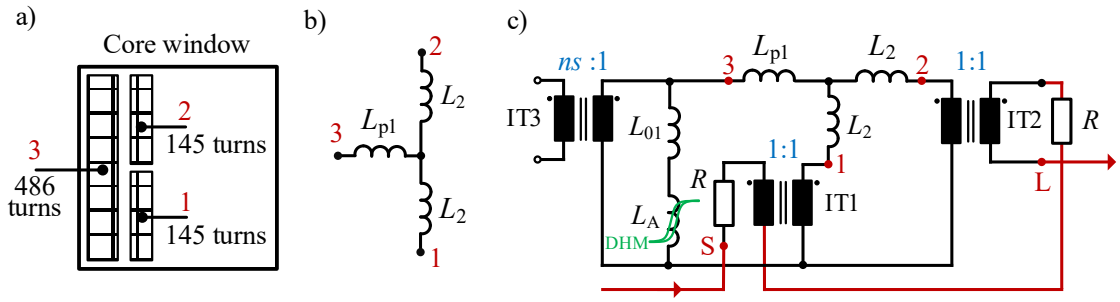


Fig. 6: Toward per-phase leakage model of the SU transformer: a) winding configuration, b) leakage model and c) model implementation.

The value of L_{01} in the models is the main parameter determining the inrush current upon transformer energization. In the model of Fig. 6c) the initial value of L_{01} can be taken as L_{p1} / 2 [8]. Their actual values are found when modeling inrush current events.

As in conventional transformer modeling, the ideal transformers (ITs) in the model of Fig. 5 are used to reproduce the voltage transformations occurring in the specific three-winding transformer. In the case of the PST, varying the IT turns ratio enables simulation of different OLTC positions.

Regardless of the voltage V_{SL} between nodes S and L in Fig. 6c), it is approximately equally divided between the ideal transformers IT1 and IT2. This indicates that the DHM inductor is subjected to a maximum voltage of $V_{SL}/2$ and, therefore, is specified with 145 turns. Consequently, the value of ns in the turns ratio of IT3 is 486 / 145, where 486 is the number of turns in the delta winding located on the left side of IT3. The following IT turns ratios, shown in TABLE 2, were used in numerical experiments.

The EU has four windings per leg, as depicted in Fig. 7. To simplify the model, the outer FW and CW windings are combined into a regulating winding RW (CW + FW) as proposed in [9]. To reproduce electrical network contained all four windings, a method of the magnetic coupling can be employed [10].

TABLE 2: IT TURN RATIOS FOR TOPOLOGY MODEL.

IT ratio	ns	ne	n
Value	$\frac{\mathrm{EWS_I}}{\mathrm{SW_S}} = \frac{486}{145}$	$\frac{\mathrm{TW}}{\mathrm{EW}} = \frac{27}{321}$	$\frac{\mathrm{CW+FW}}{\mathrm{EW}} = \frac{(98 \pm 14 \cdot k + 10^{-6})}{321}$ for k = -7 to 7
	3.351	0.0841	0.00 to 0.6106

4. CORE MODELING

To validate the electromagnetic topological model of the PST, the following sections compare real-world measurements from no-load (NL) and zero-sequence (Z0) tests with simulation results generated with three computational environments: MATLAB/Simulink in section A, followed by ATPDraw in section B, and RelaySimTest in section C.

Fig. 7 illustrates the schematic layout of the winding arrangement for both the SU and EU. The associated core cross-sections and physical dimensions are provided in TABLE 3. The electrical and nameplate parameters of the PST are listed in TABLE 7. The variables A correspond to the effective core cross-section areas of the main leg (A_L), main yoke (A_Y) and return leg (A_{LR}), additionally, C represents the return leg width, D the main leg width, E the main yoke length, F the return yoke length and H the return and main yoke width.

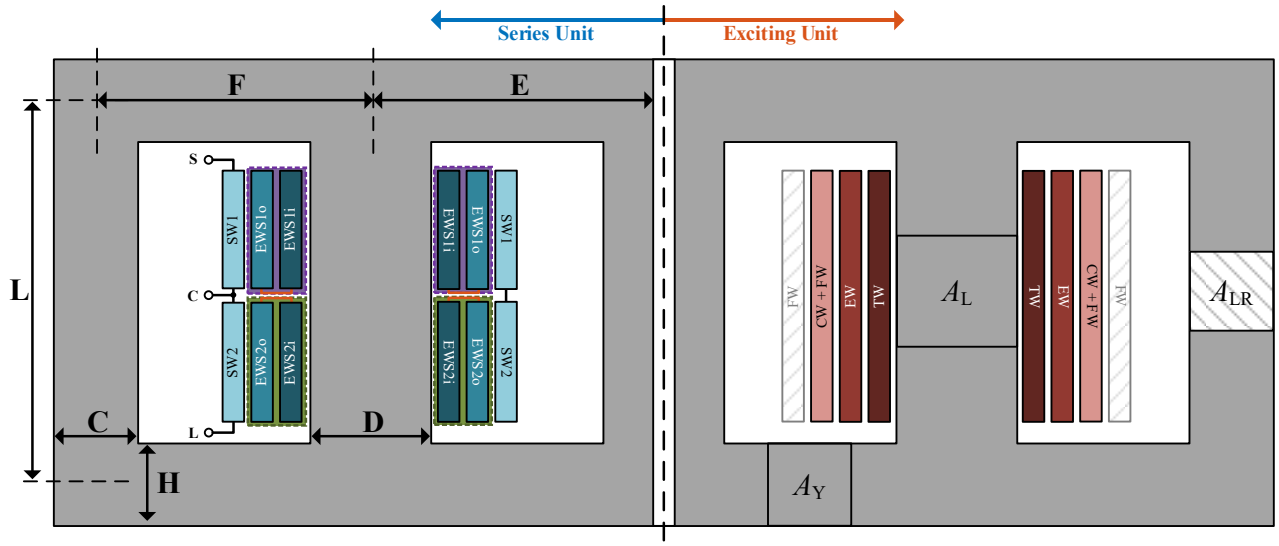


Fig. 7: Winding arrangement and core geometry of the PST SU and EU, including relevant dimensions and cross-sectional areas for simulation. The winding simplification used in the modeling is shown in SU in violet (EWS1o + EWS1i) and in green (EWS2o + EWS2i). The orange bracket shows the serial connection of EWS windings (inner and outer). The simplification in the EU is represented by the merging of CW and FW. Normally, FW represents the fourth outermost winding, highlighted in grey.

TABLE 3: CORE GEOMETRY AND DIMENSION OF PST.

Component Description	SU	EU
Effective core cross-section area of the main leg (A_L)	0.8350 m²	1.253 m²
Effective core cross-section area of the main yoke (A_Y)	0.4757 m²	0.7136 m²
Effective core cross-section area of the return leg (A_{LR})	0.4187 m²	0.6278 m²
Mean length main leg (L)	3.484 m	3.364 m
Mean length main yoke (E)	2.186 m	2.076 m
Mean length return yoke (2F+L)	2.781 m	2.809 m

4.1 Modified Jiles-Atherton (JA) Hysteresis Model in MATLAB/Simulink

The initial modeling of the PST was conducted in MATLAB/Simulink, utilizing the anhysteretic curve and JA model parameters to perform both NL and Z0 test simulations. The topology used is illustrated in Fig. 5. To investigate the fundamental function of the PST, the phase angle α_0 under NL conditions between the supply voltage V_S and the output voltage V_L was examined at the neutral position 1 of the OLTC and the two extreme positions, 29 advanced (A) and 29 retard (R). The phase angle α_0 is + 0.09° in position 1 and ± 35.02° in positions 29A and 29R, respectively, resulting in a maximum deviation of 0.09°.

During the NL test at the FAT, the PST was energized via the TW of the EU at OLTC position 1. The same setup was used for the following simulation studies. Fig. 8 compares measurements from the FAT with simulation results generated in MATLAB/Simulink. The simulated waveforms (solid lines) closely mirror the experimental data (dashed lines), validating the use of an anhysteretic curve modelled from the PST's DC hysteresis characteristics to replicate actual operating conditions.

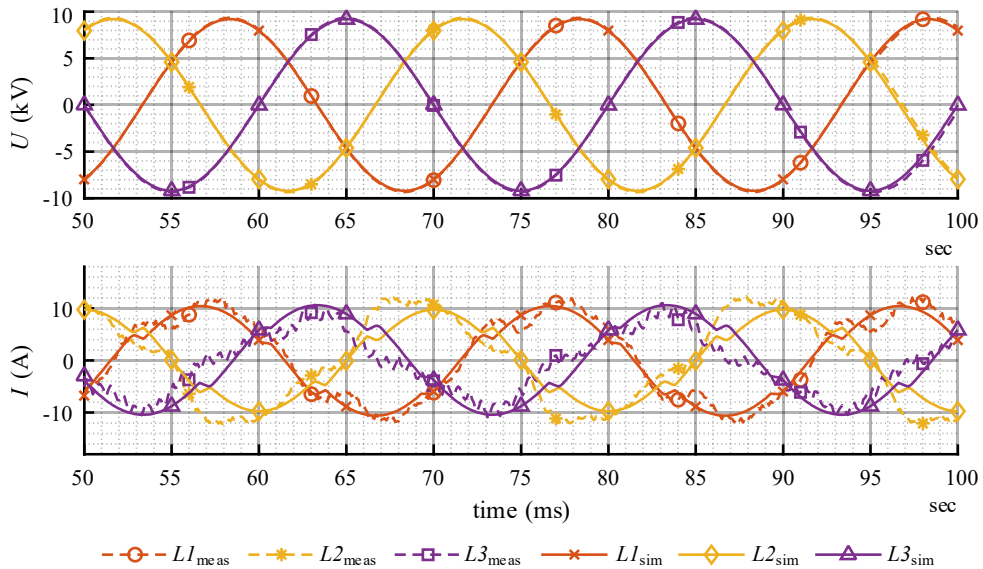


Fig. 8: Comparison between simulated (solid) and measured (dashed) waveforms during NL operation. The model utilizes a voltage-dependent inductor with a *Φ-i* characteristic derived from DC hysteresis measurement.

In the following simulation, the voltage-dependent inductors are replaced by JA hysteresis elements. To optimize the model parameters *M*s, *a*, *α*, *k* and *c* of the JA hysteresis model, the Nelder-Mead Simplex algorithm was applied as an optimization tool [11]. This allowed for the alignment of simulated phase currents with the actual terminal data gathered during DC hysteresis testing, with the entire model in MATLAB/Simulink. The optimized JA hysteresis model parameters are listed in TABLE 4.

TABLE 4: OPTIMIZED JA HYSTERESIS MODEL PARAMETERS.

*M*s	a	*α*	k	c
$2.97 \cdot 10^{6}$	329.34	$3.52 \cdot 10^{-4}$	15.19	0.29

The simulated currents obtained with the JA hysteresis model (average RMS value 8.8 A) are shown in Fig. 9. Compared to the simulation results using the *Φ-i* characteristic (average RMS value 8.4 A) in Fig. 8, the phase currents show a waveform that is slightly less accurate. Although the JA model is theoretically better suited to more accurately capture hysteresis effects, the model implementation relies on simplifications that lead to the observed deviations in the simulated current waveforms. Consequently, the anhysteretic model currently shows better agreement with the measured data. Future optimizations of the JA model, particularly with regard to the detailed consideration of winding geometries and parasitic capacitances, will be necessary to capture the NL current waveforms more accurately.

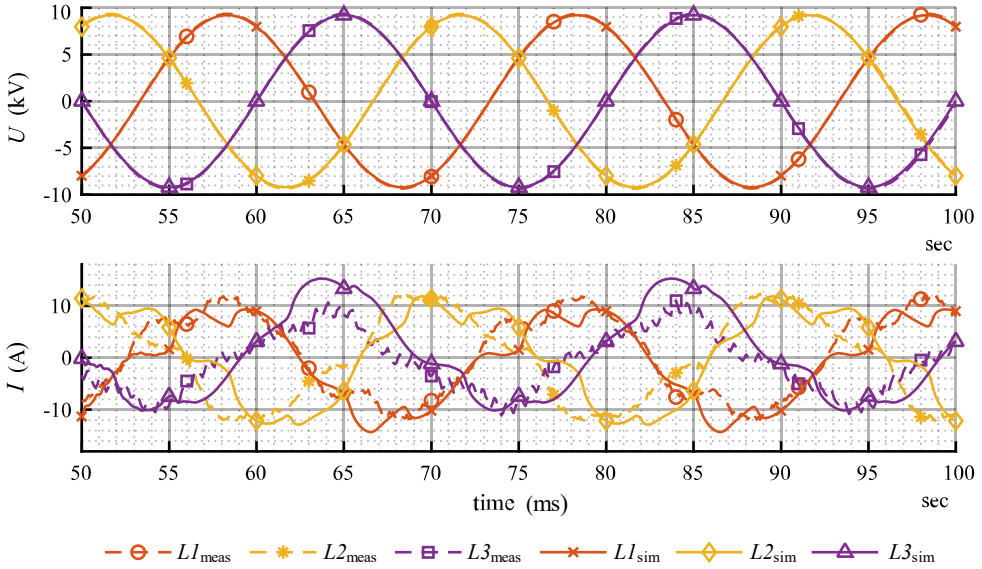


Fig. 9: Comparison of calculated and measured NL voltage and current waveforms using the JA hysteresis model.

The Z0 test was conducted using both the anhysteretic and JA models. The resulting NL current waveforms prove near-perfect alignment with the FAT measurements.

4.2 ATPDraw model

The topological model of the PST can be implemented in various software environments. ATPDraw is attractive because it includes the dynamic hysteresis model (DHM), available in ATP/ATPDraw since version 7.3 (2019). There is no need to use loss resistors in conjunction with the DHM inductors, since they reproduce all three components of the total core loss, namely static (hysteretic), classical eddy-current, and excess losses. The use of the DHM in ATPDraw model of the PST is illustrated in Fig. 10, which shows *B*-*H* trajectory of leg A of the EU during the NL test. To initialize the ATPDraw model for the NL test, a ramped voltage is applied to the Y1-Y3 terminals of the TW (EU). This explains the *B*-*H* spiral curve shown in Fig. 10.

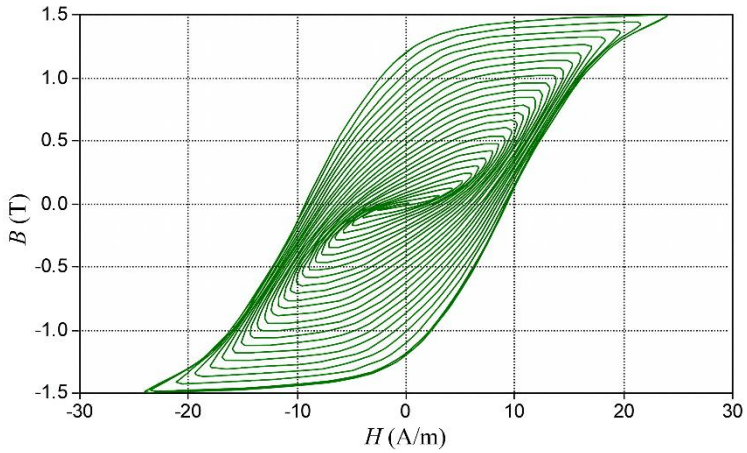


Fig. 10: Untwisting dynamic *B*-*H* spiral for the Leg A of EU.

The simulated no-load line currents from ATPDraw, along with their average RMS value (8.6 A), are presented in Fig. 11. Although the FAT NL test yielded a measured average RMS value of 7.1 A, the discrepancy is acceptable. This minor difference is due to the fact that PST terminal capacitances were neglected in the calculation. Subsequent NL simulations demonstrated that terminal capacitances have a significant impact on the overall results. It is essential to consider these parameters, given their critical role in ferroresonance investigations and the modeling of high-frequency processes [6].

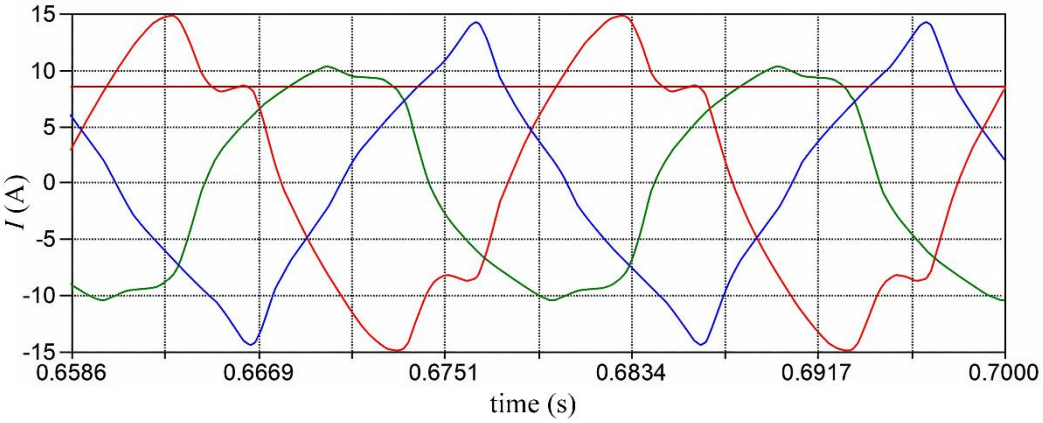


Fig. 11: Line currents at no-load and their average RMS value (horizontal) predicted by the DHM-based ATPDraw model.

The ATPDraw model was also employed to simulate the PST model in Fig. 5. Three-phase equivalent of the supply network was connected to terminals S1, S2 and S3. Large wye-connected resistors were connected to terminals L1, L2 and L3 to simulate no-load mode. Fig. 12 shows phase angle α_0 versus the turns ratio n calculated for both positions of the Advanced-Retard Switch (ARS).

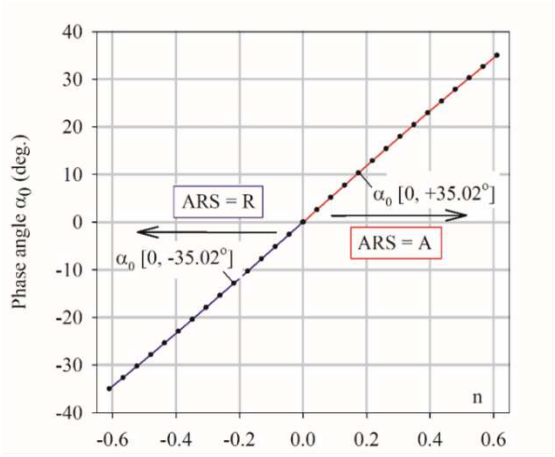


Fig. 12: Phase angle α_0 under no-load vs. n.

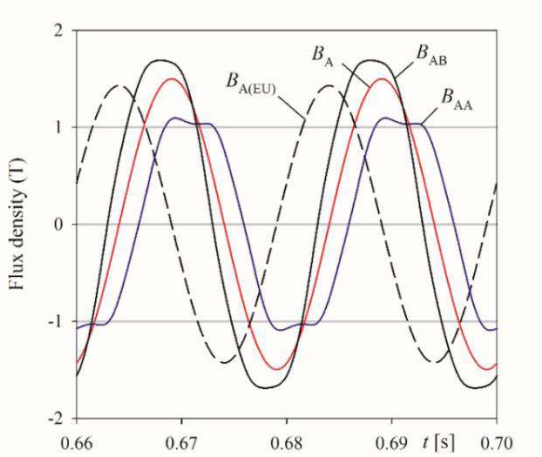


Fig. 13: Flux density waveforms in the SU and EU.

Fig. 13 illustrates the possibilities of the DHM-based model in predicting flux densities in the cores of the SU and EU transformers. The waveforms in Fig. 13 were calculated for maximum value of n: sinusoidal B_A is the flux density in the SU leg A, while B_{AB} and B_{AA} represent flux densities in the yoke AB and the side limb AA of the SU. Flux densities B_A, B_{AB} and B_{AA} diminish to zero when n approaches 0. In contrast, the induction in the leg A of the EU (dashed curve $B_{A(EU)}$) is virtually independent of n. Knowing the flux densities in the cores and yokes of both transformers enables the determination of core losses and their variation with the PST operating mode.

4.3 RelaySimTest

RelaySimTest is a power system simulation software intended for testing protection relays, either individually or as part of a complete system with multiple relays operating simultaneously. It uses transient analogue signals that are directly injected into the relays by test sets. High priority was given to usability for electrical engineers; therefore, complex power system components are defined using widely available data, such as transformer nameplate information. The software automatically performs the internal calculations of system elements, and the user cannot modify the underlying assumptions. The PST example shown in Fig. 1 is reproduced is reproduced in RST using three magnetically coupled windings, with all terminals accessible for the external connection of open-winding elements (Fig. 14a)). The windings are formed as follows:

- SU windings: the primary (P) and the secondary (S) are connected in series to represent the SW (III) of the PST, while the tertiary (T) is connected in delta. To realize the SU delta connection, a phase permutation element is used. By switching its position between 'A' and 'R', the delta configuration can be altered from d3 to d9, thereby reversing the quadrature voltage orientation by 180°.
- EU is modelled in RST software as a two-winding YNyn0 transformer, with a tap changer placed on the secondary (S) side. In the proposed model the linear regulation of the voltage (indirect phase-shift regulation) is used by a single tap changer, while the details of coarse and fine winding are not explicitly considered.

The SU and EU transformers are interconnected according to the topology of symmetrical dual-core PST with use of second phase permutation element.

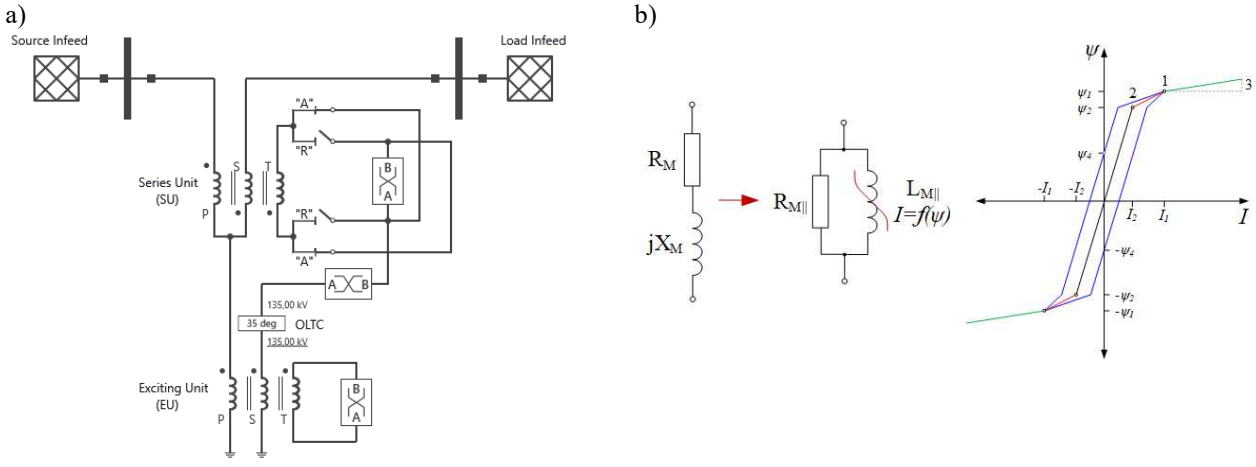


Fig. 14: RelaySimTest a) PST model and b) magnetization characteristic with model hysteresis.

To parametrize the PST, it is necessary to provide the following data for individual PST units (SU and EU):

- Elements of the main branch and magnetization (linear part) of the transformer for each individual winding: rated voltage V_r, reference apparent S_ref, SC voltage $u_\mathrm{sc\%}$ in percent related to the nominal voltage, ohmic losses during SC impedance test $P_\mathrm{loss,sc}$ or relative real part of the SC voltage $u_\mathrm{Rsc\%}$ related to the nominal voltage, percentage no load current I_NL refereed to the nominal current and core type (three or five leg).
- For magnetization branch non-linear elements:
  - final flux saturation ψ_1, relative to the base flux ψ_base,
  - saturated inductance L_sat relative to the leakage inductance (internally calculated from the SC impedance),
  - and for hysteresis maximum residual flux ψ_4 in percent of the start saturation.

Hence the main objective of the paper is placed in the non-linear aspects, thus here only the part reflected in this objective is provided. Detailed documentation about other aspects of PST modeling in RelaySimTest is provided in [12].

Linear elements defining the magnetizing branch (Fig. 14 (b)) are the $R_\mathrm{M} + \mathrm{j}X_\mathrm{M}$ which are described by (1):

$$R_\mathrm{M} = \frac{100}{I_\mathrm{NL}} \frac{3V_\mathrm{r}^2}{S_\mathrm{ref}} \cos(75°) \qquad \text{and} \qquad \mathrm{jX_M} = \frac{100}{I_\mathrm{NL}} \frac{3V_\mathrm{r}^2}{S_\mathrm{ref}} \sin(75°) \tag{1}$$

For representation of non-linear elements of magnetizing branch, the resistance $R_{\mathrm{M}\|}$ and the unsaturated inductance L_unsat are chosen to be equivalent to the impedance $R_\mathrm{M} + \mathrm{j}X_\mathrm{M}$ at the rated frequency f_R:

$$R_{\mathrm{M}\|} = \frac{R_\mathrm{M}^2 + X_\mathrm{M}^2}{R_\mathrm{M}} \qquad \text{and} \qquad L_\mathrm{unsat} = \frac{R_\mathrm{M}^2 + X_\mathrm{M}^2}{2\pi f_\mathrm{R} X_\mathrm{M}} \tag{2}$$

Magnetization characteristic (Fig. 14 b)) is defined by three linear segments. The slopes of these segments determine the magnetizing branch inductance $L_{\mathrm{M}\|}$:

$$\begin{array}{rcl} \psi \le \psi_2 & \rightarrow & L_{\mathrm{M}\|} = L_\mathrm{unsat} \\ \psi_2 \le \psi \le \psi_1 & \rightarrow & L_{\mathrm{M}\|} = L_\mathrm{knee} \\ \psi > \psi_2 & \rightarrow & L_{\mathrm{M}\|} = L_\mathrm{sat} \end{array} \tag{3}$$

The base flux ψ_Base is a peak value for the flux reached in the transformer magnetizing branch in steady state when the magnetizing branch is excited with the rated voltage V_r (with respect to the winding connection w: 1 for delta and 1/√3 for Wye) at the rated frequency f_r:

$$\psi_\mathrm{base} = \frac{\sqrt{2} V_\mathrm{r} w}{2\pi f_\mathrm{r}} \tag{4}$$

RelaySimTest automatically calculates the inductance of a "knee" region as follows L_knee:

$$L_\mathrm{knee} = \frac{L_\mathrm{unsat}}{10} \tag{5}$$

The Saturated inductance L_sat (Fig. 14 b) point 3) is relative to the minimum value of the leakage inductance of windings: Primary to Secondary (X_{PS}), Primary to Tertiary (X_PT) and Secondary to Tertiary (X_ST).

$$L_\mathrm{Sat} = \frac{\min(X_\mathrm{PS}, X_\mathrm{PT}, X_\mathrm{ST})\, L_\mathrm{sat}}{2\pi f_\mathrm{R}} \tag{6}$$

The models are validated by comparing three-phase NL and SC measurements with the computed transient current waveforms. The individual device data for the PST model is listed in TABLE 5, while TABLE 6 provides an overview of the verification parameters simulated in the software RelaySimTest, additional PST values are taken from FAT report.

TABLE 5: PST INDIVIDUAL UNITS DATA FOR MODEL IN RelaySimTest.

PST Unit	Parameter	Description	Value
SU	Rated voltage	Primary winding (Series)	40.278 kV
		Secondary winding (Series)	40.278 kV
		Tertiary (delta)	135.00 kV
	Reference power	Primary winding (Series) Secondary winding (Series) Tertiary (delta)	600 MVA
	Short circuit voltage at reference power	Primary - Secondary	
		Primary - Tertiary	53.23 %
		Secondary - Tertiary	
	No load current		0.37 %
EU	Rated voltage	Primary winding	127.75 kV
		Secondary winding	77.943 kV
		Tertiary	123.00 kV
	Reference power	Primary winding Secondary winding Tertiary	600 MVA
	Short circuit voltage at reference power	Primary - Secondary	16.48 %
		Primary - Tertiary	0.16 %
		Secondary - Tertiary	16.48 %
	No load current		0.44
	Tap changer voltage for 35°		135.00 kV
	Tap changer voltage for 17.9°		67.73 kV
	Tap changer voltage for 0.0°		0.20 kV*

*Minimum voltage allowed by the software. Under real-world conditions, the voltage is 0.00 kV.

TABLE 6: VERIFICATION PARAMETER OVERVIEW FOR THE SOFTWARE RELAYSIMTEST (RST Model).

	ARS & tap position	No-Load Current	No-Load α_0 phase angle	Short-Circuit Positive Z_{SC}	Short-Circuit Z_0
PST	MAX A/R	11.84 A	+35.0° / -35.0°	17.04 Ω	13.35 Ω
	MID A/R	NA	+17.9° / -17.9°	13.81 Ω	13.35 Ω
	MIN	7.15 A	+0.0°	12.95 Ω	13.35 Ω
RST Model	MAX A/R	11.81 A	+35° / -35°	17.034 Ω	13.36 Ω
	MID A/R	8.40 A	+17.9° / -17.9°	14.053 Ω	13.36 Ω
	MIN	7.12 A	+0.05°	12.953 Ω	13.36 Ω
	deviation	-0.25%	0.05°	1.92%	0.07%

5. CONCLUSION

This paper examines a case study in which a 600 MVA five-legged PST was modelled using various methods for electromagnetic transients in the low-frequency range. Precisely representing the electromagnetic characteristics of a PST continues to be a high difficulty. This is especially true for in-service equipment, where technical details about the core design are missing. This study proves that a reliable electromagnetic model of PSTs can be built even with minimal geometric data and the use of a DC hysteresis measurement. The conducted models enable the simulation of low-frequency transients, such as inrush currents and saturation caused by DC bias, without the need for comprehensive manufacturer specifications.

A major difficulty in modeling the PST lies in the accurate determination of the inductances of the individual windings, as the SC test in the FAT is only performed on one winding. To improve the PST model further, future work will need to distinguish more clearly between the DC hysteresis effects of the two separate cores (SU and the EU). Testing the magnetic behavior of these units individually before the assembly would provide a better base for electromagnetic modeling. By conducting SC tests from each side of the winding, the specific leakage inductances can be identified more accurately, leading to a more precise overall model. Another improvement is to modify the topology-based model to include a fourth winding. This means that the simplification of CW + FW to RW used in the paper is no longer necessary and the actual winding arrangement can be used.

Additionally, future research will concentrate on investigating inrush currents, over-excitation, and the impact of DC bias on the PST. This will also involve a detailed study of the non-linear joint air gap [13] to further refine the model's accuracy.

6. REFERENCES

1. Martinez JA, Mork BA (2005) Transformer Modeling for Low- and Mid-Frequency Transients—A Review. IEEE Trans Power Deliv 20:1625–1632. https://doi.org/10.1109/TPWRD.2004.833884

2. Fuchs EF, You Y (2002) Measurement of Psi-i characteristics of asymmetric three-phase transformers and their applications. IEEE Power Eng Rev 22:69–70. https://doi.org/10.1109/MPER.2002.4312518

3. Albert D, Maletic D, Renner H (2021) Measurement based transformer modelling approach. In: ETG Congress 2021. pp 1–6

4. Cherry EC (1949) The Duality between Interlinked Electric and Magnetic Circuits and the Formation of Transformer Equivalent Circuits. Proc Phys Soc Sect B 62:101–111. https://doi.org/10.1088/0370-1301/62/2/303

5. Zirka SE, Albert D, Moroz YI, Renner H (2022) Further Improvements in Topological Transformer Model Covering Core Saturation. IEEE Access 10:64018–64027. https://doi.org/10.1109/ACCESS.2022.3183279

6. Krämer A, Ruff J (1998) Transformers for phase angle regulation considering the selection of on-load tap-changers. IEEE Trans Power Deliv 13:518–525. https://doi.org/10.1109/61.660923

7. Jazebi S, Rezaei-Zare A, Lambert M, et al (2016) Duality-Derived Transformer Models for Low-Frequency Electromagnetic Transients—Part II: Complementary Modeling Guidelines. IEEE Trans Power Deliv 31:2420–2430. https://doi.org/10.1109/TPWRD.2016.2556686

8. Høidalen HK, Mork BA, Gonzalez F, et al (2009) Implementation and verification of the Hybrid Transformer model in ATPDraw. Electr Power Syst Res 79:454–459. https://doi.org/10.1016/j.epsr.2008.09.003

9. Stadler J (2012) Modellierung eines Phasenschiebertransformators unter Berücksichtigung von Sättigungserscheinungen im Eisenkern: Masterarbeit. Master Theses, Graz University of Technology

10. Alvarez-Marino C, de Leon F, Lopez-Fernandez XM (2012) Equivalent Circuit for the Leakage Inductance of Multiwinding Transformers: Unification of Terminal and Duality Models. IEEE Trans Power Deliv 27:353–361. https://doi.org/10.1109/TPWRD.2011.2173216

11. Lagarias JC, Reeds JA, Wright MH, Wright PE (1998) Convergence Properties of the Nelder-Mead Simplex Method in Low Dimensions. SIAM J Optim 9:112–147. https://doi.org/10.1137/S1052623496303470

12. Bednarczyk T (2022) Phase Shifting Transformer Protection Test with System-based Approach

13. Zirka SE, Moroz YI, Chiesa N, et al (2025) Alternative Techniques in Simulating Transformer No-Load Characteristics and Inrush Currents by Circuit Models. IEEE Access 13:211796–211808. https://doi.org/10.1109/ACCESS.2025.3643152

STATEMENTS AND DECLARATIONS

Competing Interests: The authors declare that they have no competing interests, financial or non-financial, that are directly or indirectly related to the work submitted for publication.

APPENDIX

TABLE 7: PST TECHNICAL DATA.

Component Description	Variable	Value(s)
Vector Group		Ynyn/IIId S0-3/
Nominal Voltage		
Voltage S/L	$V_{S/L}$	232 kV
Voltage tertiary winding (OLTC: 1)	V_{TW}	11266 V
Rated Current	I_R	1493 A
Short Circuit Impedance (referred to 600 MVA)		total losses | phase current | phase-to-phase voltage | SC voltage in percent related to nominal voltage
OLTC 1		700.5 kW | 1466 A | $U_k = 33506$ V | u_k=14.44 %
OLTC 29A		1326.0 kW | 1493 A | $U_k = 44067$ V | u_k=18.99 %
OLTC 29R		1350.9 kW | 1493 A | $U_k = 44018$ V | u_k=18.97 %
No-Load Losses		Active Power | Apparent power
OLTC 1 at 11266 V (100%)		106.2 kW | 140.0 kVA
OLTC 1 at 12393 V (110%)		135.8 kW | 161.1 kVA
OLTC 29A at 10747 V (100%)		197.2 kW | 220.2 kVA
OLTC 29A at 11822 V (110%)		250.3 kW | 261.0 kVA
Zero-Sequence Impedance		
Z_S | OLTC: 1 (neutral) | S1-S2-S3 connected vs. Np; Y3 grounded; L1, L2, L3, Ns, Y1, Y2, Y4 open	ZS1	2170.48 V | 487.87 A | 50.10 kW | $Z_0 = 14.88$ % $Z = 13.35\ \Omega$ | $R = 0.63\ \Omega$ | $X = 13.33\ \Omega$
Z_S | OLTC: 29A (advanced) | S1-S2-S3 connected to Np; Y3 grounded; L1, L2, L3, Ns, Y1, Y2, Y4 open	ZS29A	2113.23 V | 474.92 A | 47.12 kW | $Z_0 = 14.88$ % $Z = 13.35\ \Omega$ | $R = 0.63\ \Omega$ | $X = 13.33\ \Omega$
Z_S | OLTC: 29R (retard) | S1-S2-S3 connected to Np; Y3 grounded; L1, L2, L3, Ns, Y1, Y2, Y4 open	ZS29R	2236.42.23 V | 502.57 A | 52.93 kW | $Z_0 = 14.88$ % $Z = 13.35\ \Omega$ | $R = 0.63\ \Omega$ | $X = 13.34\ \Omega$
Winding Capacitance		
$C_{SU\text{-}GND}$	$C_{S/L,SU\text{-}GND}$	12858.8 pF
$C_{EU\text{-}GND}$	$C_{S/L,EU\text{-}GND}$	21381.9 pF
$C_{TW\text{-}GND}$	$C_{TW\text{-}GND}$	30574.2 pF
Winding Resistances		A | B | C
Winding resistance SW_S in Ω (at 75° C)	R_{SWS}	0.028514 | 0.028474 | 0.0258528
Winding resistance SW_L in Ω (at 75° C)	R_{SWL}	0.028527 | 0.028467 | 0.028546
Winding resistance EW in Ω (at 75° C)	R_{EWS}	0.165400 | 0.165387 | 0.165178
Winding resistance CW (at 75° C, OLTC:29A/R)	R_{CW}	0.112302 | 0.113478 | 0.113084
Winding resistance FW in Ω (at 75° C, OLTC:1)	R_{FW}	0.001234 | 0.001201 | 0.001213
Winding resistance EW in Ω (at 75° C)	R_{EW}	0.114699 | 0.114788 | 0.114777
Winding resistance TW in Ω (at 75° C)	R_{TW}	0.007766 | 0.007299 | 0.007122
Turns		
Turns per SW	Nsw	$2 \cdot 145$
Turns per EWS (EWS_{1i} & EWS_{2i})	N_{EWSi}	$2 \cdot 251$
Turns per EWS (EWS_{1o} & EWS_{2o})	N_{EWSo}	$2 \cdot 235$
Turns per FW	N_{FW}	$\pm 14 \cdot 7$
Turns per CW	N_{CW}	98
Turns per EW	N_{EW}	321
Turns per TW	N_{TW}	27